



Research Article

Antimicrobial, Antioxidant and T47D Cytotoxic Activities of *Trichaptum* sp., A Fungal Endophyte from *Phyllanthus niruri* Linn.: *In vitro* and *in silico* Studies

¹Rollando Rollando and ²Maywan Hariono

¹Program of Pharmacy, Faculty of Science and Technology, Ma Chung University, 65151 Malang, Indonesia

²Faculty of Pharmacy, Sanata Dharma University, Maguwoharjo, Sleman, 55282 Yogyakarta, Indonesia

Abstract

Background and Objective: Fungal endophyte is a good source in producing bioactive compounds possessing antibacterial, antioxidant and anticancer activities. This study was aimed to produce fungal endophyte from *Phyllanthus niruri* and to test its *in vitro* bioactivity as antibacterial, antioxidant and cancer cytotoxic agent. The molecular mechanism of the fungal activities was then predicted using *in silico* docking. **Materials and Methods:** Fungal endophyte from genus *Trichaptum* sp., isolated from *Phyllanthus niruri* herbs was extracted using ethyl acetate and further fractionated using n-hexane, diethyl ether and ethanol and ethanol 96% through chromatography column ready for testing. The antimicrobial test was carried out using disc diffusion method. The antioxidant was determined using hydrogen peroxide free radical scavenging and reducing power capacity. The cytotoxicity assay against T47D breast cancer cell was carried out using (3-(4,5-dimethylthiazol-2-yl)-2,5-diphenyltetrazolium bromide) method. The docking of chemicals reported in the sample was performed using AutoDock Vina. **Results:** Diethyl ether fraction was the most active fraction against *Escherichia coli* and T47D cell growth in a non-toxic dose, whereas the best antioxidant activity was performed by ethanol 96% fraction. Assays on the cell cycle modulation and its apoptotic behavior suggested that the T47D was disrupted via p53 mutant, Bcl-2 and NF- κ B abrogation. Molecular docking of compounds identified in the fraction suggested that these activities could belong to the maltose binding periplasmic and oxydosqualene cyclase inhibition in *Escherichia coli* and T47D, respectively. **Conclusion:** Fungal endophyte from *Phyllanthus niruri* was successfully isolated as genus *Trichaptum* sp. and serving as antibacterial, antioxidant and anticancer activities.

Key words: Fungal endophyte, *Trichaptum* sp., *Phyllanthus niruri*, biological activities, molecular docking

Received:

Accepted:

Published:

Citation: Rollando Rollando and Maywan Hariono, 2016. Antimicrobial, antioxidant and T47D cytotoxic activities of *Trichaptum* sp., a fungal endophyte from *Phyllanthus niruri* Linn.: *In vitro* and *in silico* studies. Asian J. Cell Biol., CC: CC-CC.

Corresponding Author: Rollando Rollando, Program of Pharmacy, Faculty of Science and Technology, Ma Chung University, Malang 65151, Indonesia
Tel: +62341550171 Fax: +62341550175

Copyright: © 2016 Rollando Rollando and Maywan Hariono. This is an open access article distributed under the terms of the creative commons attribution License, which permits unrestricted use, distribution and reproduction in any medium, provided the original author and source are credited.

Competing Interest: The authors have declared that no competing interest exists.

Data Availability: All relevant data are within the paper and its supporting information files.

INTRODUCTION

Endophytes are microsize particles symbiotically living in between xylem and phloem, leaves, roots, fruits and stems¹. A fungal endophyte was known to produce some biological active compounds such as alkaloid, terpenoid, phenol, etc.², demonstrating antioxidant, anticancer, antibacterial, antiviral, antifungal and antileishmanial activities³. Previously, *Phyllanthus amarus* Schum. and Thonn. was identified depositing classes of endophytic fungi and bacteria, which lived in between plant cells⁴. There have been a few recent studies utilizing fungal endophyte as the sources of bioactive compounds from plants and alga such as *Pinus strabus*⁵, *Flabellia petiolata*⁶, *Nerium indicum*⁷, *Taxus*⁸ and *Hydrastis canadensis*⁹. The fungal endophyte was indicated as much as 10 types in *Phyllanthus amarus*, therefore, this herb has been reported as the resource in producing a fungal endophyte implemented in drug developments with various biological activities¹⁰.

In the same family of *Phyllanthaceae*, *Phyllanthus niruri* Linn., also has a potential to be a new source for producing a fungal endophyte. Originally, this herb contains chemical substances including lignin, glycoside, alkaloid, ellagitannin, terpene, phenylpropanoid, flavonoid, imidazole and polyphenol^{11,12}. Instead of this herb has been studied its pharmacological activity in the treatment of bladder infection, as immunomodulator, anti-inflammatory and antiviral agents^{13,14} to date, there is no report about this species to be used as an endophyte source. Hence, it is interesting to study more about an extraction and biological evaluations of the fungal endophyte from this species.

Bacteria resistances in some antibiotics need a high concern in discovering and developing new antibacterial which are more susceptible to the mutant and selective to eradicate the bacteria cells with no effects to the host¹⁵. Subsequently, antioxidant is currently become a hot topic related with an oxidative stress and a cell damage, indicating some diseases such as a cancer and coronary heart disorder¹⁶. Furthermore, a searching of an anticancer that is less toxic has been a lengthy challenge with no results is perfectly killing the cancer cells without affecting the normal ones¹⁷. In this present study, it was explore the opportunities of *Phyllanthus niruri* as the new source for mining the fungal endophyte in organic fractions such as n-hexane, diethyl ether and ethanol. These fractions were further studied its *in vitro* antibacterial, antioxidant and anticancer activities due to its cytotoxicity effects towards T47D breast cancer cells. Furthermore, the modulation of a cell cycle leading to apoptosis by the most active fraction on the T47D was also

investigated. The fungal endophyte was characterized using both microscopic and molecular genetic analysis to confirm the genus of the endophyte. Meanwhile, the compounds contained in the most active fraction were identified using Gas Chromatography-Mass Spectroscopy (GC-MS).

In rational drug designs, the proteins which are responsible towards the pathogenesis can be used as the target in combating the microorganism as well as the malign cells. Although we have not tested the fractions against cells at protein levels due to our limitations, however, it was tried to gain insight mechanisms of identified compounds in the endophyte against a diverse protein been expressed in the most susceptible bacteria and the T47D using molecular docking.

MATERIALS AND METHODS

Phyllanthus niruri leaves were collected from Materia Medica, Malang, Indonesia with No. of specimen MN 02371. Potato Dextrose Broth (PDB) was prepared from potatoes collected from Batu, Malang. Dextrose, muller hinton, Potato Dextrose Agar (PDA), Nutrient Agar (NA) and nutrient broth were purchased from Merck. The microbes were *Escherichia coli* K-12, *Staphylococcus aureus* NCTC 8325 and *Salmonella thypi* Ty2 purchased from Microbiology Laboratory, Brawijaya University, Indonesia. All chemicals were purchased from Merck with analytical grade i.e., sodium hypochlorite (NaOCl), ethyl acetate, n-hexane, methanol, chloroform, hydrogen peroxide, phosphate buffer pH 7.0, potassium iron (III) cyanide, iron (III) chloride, triton-X 100 and silica 60 for column chromatography. Propidium Iodide (PI) for cell cycle assay was HPLC grade (Sigma). The T47D cell and RNase was courtesy from Parasitology Laboratory of Medical Faculty, Gadjah Mada University, Indonesia. Dulbecco's Modified Eagle Media (DMEM), Fetal Bovine Serum (FBS), penicillin-streptomycin, fungizone and trypsin-EDTA were purchased from Gibco, whereas tissue culture dish was from Iwaki. Nucleon PHYTOpure reagents and flow cytometry annexin V-FLOUS apoptosis detection kit were purchased from Amersham LIFE SCIENCE and Roche, respectively. The used instruments were autoclave (AC-300AE, Tiyoda), laminar air flow cabinet (FARRco), genetic analyzer (ABI PRISM 3130 Applied Biosystems), UV-Vis spectrophotometer (Shimadzu), GC-MS (AGILENT GC 6890N 5975B MSD), elisa reader (BioRad) and flow cytometer (FACTS).

Isolation: A surface sterilization was used for the isolation of the fungal endophyte according to Kumar *et al.*¹⁸ method. To eliminate the epiphytic microflora and parasite from the

sample's leaves, a sterile distilled water was used by washing and shaking them for 1 h. The healthy leaves were soaked using ethanol 70% for 2 min, followed by 1% of NaOCl solution for another 3 min. These were then rinsed in re-distilled and sterilized waters for a couple minutes. Leaves were dried on a blotting sheet followed by taking the imprints from the media plates. Finally, samples were chopped onto 10 mm of segment's diameter and placed them (five segments on each plate) onto petri dishes containing PDA (supplemented with 100 mg mL⁻¹ of chloramphenicol). This was then incubated at 25°C until the growth of endophytic fungi was discerned. After two weeks, hyphae were inoculated on PDA plates at 28°C for a purification. Each fungal isolate was checked for their purity and transferred into the new medium using the hyphal tip method. The mycelial tips were transferred into the PDA plates. This purification method was repeated for more than five times. Mycelia were then stored in a sterile test tube slant. One of the isolates coded as BJ was then selected for further molecular identifications.

Molecular genetic analysis: The identification of fungal isolates was carried out at a molecular level based on a partial genetic analysis at Internal Transcribed Spacer (ITS) of the fungal ribosomal DNA. The DNA isolation was initiated by growing the fungi isolate in PDB and then incubated for 72 h. A biomass of fungal mycelia was subsequently harvested for DNA extraction process. Fungal DNA was extracted using nucleon PHYTOpure reagents. The PCR amplification was carried out using primary^{19,20} ITS 4: 5'-TCCTCCGCTTAT TGATATGC-ITS 3' and Primary 5: 5'-AAAAGTAGTCGTGGAAACAAGG-3'. The PCR product was purified using PEG precipitation method²¹ followed by a cycle sequencing. The results of the cycle sequencing were purified back using ethanol purification method. The sequence of nitrogen bases was read using an automated DNA sequencer. The raw data of the sequence was then trimmed and assembled using bioedit program (<http://www.mbio.ncsu.edu/BioEdit/bioedit.html>). The assembled sequence was BLAST-ed using genomic data, which has been deposited in DDBJ/DNA Data Bank of Japan (<http://blast.ddbj.nig.ac.jp/>) or NCBI/National Center for Biotechnology Information (<http://www.ncbi.nlm.nih.gov/BLAST/>) to determine the taxon/species based on the highest homology with the reference.

Tissue culture: The colony of fungal endophytes was taken from PDA using aseptic to have 5 plugs with 0.5 cm in diameter. A volume of 200 mL of the colony was inoculated into a sterilized conical flask and then incubated at a room

temperature for 14 days. The mycelium was then collected from the filtrate by a filtration, followed by drying them at 50°C. Thereafter, the dried mycelium was then pulverized.

Extraction: The mycelium powder was macerated using ethyl acetate (1:3) for 48 h with a frequent agitation. The liquid extract was then filtrated and the residue was re-macerated using new ethyl acetate for 24 h with the same frequent agitation. The filtrate was then collected and concentrated under a reduced pressure.

Fractionation: The concentrated extract (200 mg) was then fractionated using 200 µL of each n-hexane (100%), diethyl ether (100%) and ethanol 96% through a chromatography column with an isocratic technique. Each fraction was collected and concentrated under a reduced pressure followed by drying them at 50°C.

Antimicrobial test: The antimicrobial test was carried out using a disc diffusion (Kirby-Bauer test) method²², whereas the Minimum Inhibition Concentration (MIC) was performed using a micro-dilution test²³.

Screening of active fractions: The series of concentrations for each fraction was prepared to have 100, 50, 25, 12.5 and 6.25 µg mL⁻¹ of working solutions. Ten microliters of each was dropped into a paper disc to have amounts of the isolate for each paper disc, i.e., 1000, 500, 250, 125 and 62.5 µg mL⁻¹. These were left to dry up to the paper disc being attached to the media. Streptomycin 10 mg mL⁻¹ (10 µL) and a sterile anhydrous ethanol were used as the positive and the negative control, respectively. The bacterial culture was then incubated at 37°C for 18-24 h followed by viewing the inhibition zone around the paper disc. Subsequently, the widest diameter of the inhibition zone was selected as the active fraction.

Determination of Minimum Inhibition Concentration (MIC): A volume of 50 µL of Muller Hinton media was transferred into 96-microwell plate, followed by adding 50 µL of the bacterial suspension, which have been adjusted its turbidity based on McFarland standard 0.5²⁴. This mixture was then diluted up to 10 times, therefore, the final concentration would be 250, 125, 62.5, 31.25, 15.63, 7.81 and 1.96 µg mL⁻¹. Streptomycin 10 mg mL⁻¹ was used as the positive control. The sample was then incubated at 37°C for 18-24 h and the cell density was measured as absorbance using microplate reader at 595 nm. The absorbance were converted into percentage inhibition and then extrapolated against the

concentration of the active fraction. The IC_{50} of the fraction was then calculated and analyzed according to Probit analytical method managed by Minitab software (www.minitab.com). The MIC measurement was performed by pipetting 3 μ L of the solution from each well to be streaked on the NA without adding the microbes and working solution. If only the streaked media being clear after 18-24 h of the incubation at 37 °C, the MIC value was defined.

Determination of a total phenolic content: The total phenolic content was determined using Folin-Ciocalteu reagent with galic acid as the reference²⁵. Each of fractions was dissolved into methanol to have 2 mg mL^{-1} of concentration followed by adding 500 μ L of Folin-Ciocalteu (50%) and 2 μ L of Na_2CO_3 20%. This mixture was top up with 5 μ L of distilled water and then stored at a room temperature for 20 min, followed by reading its absorbance at 765 nm. The total phenolic content was observed based on the absorbance to the linear regression equation generated from the galic acid standard curve (30, 45, 60, 75 and 90 μ g mL^{-1}).

Determination of antioxidant activities: Two methods were used in determining the antioxidant activities of the fractions, i.e., hydrogen peroxide free radical scavenging³ and reducing power capacity²⁶.

Hydrogen peroxide free radical scavenging: A solution of hydrogen peroxide (40 mmol L^{-1}) was prepared using phosphate buffer pH 7.5. The fraction was dissolved into a distilled water to have 2 mg mL^{-1} of concentration and then added with H_2O_2 solution. After 10 min of the reaction, the sample was read its absorbance at 230 nm. The capacity of the fraction to scavenge the H_2O_2 radical was calculated based on the formula as followed:

$$\text{Scavenging capacity (\%)} = \frac{(A_i - A_t)}{A_i} \times 100$$

where, A_i is absorbance of the control and A_t is absorbance of the sample.

Reducing power capacity: Each of fractions was dissolved into 1 mL of a distilled water and then mixed up with 2.5 mL of phosphate buffer pH 6.6 and 2.5 mL of potassium iron (III) cyanide 1% w/v. The mixture was then centrifuged at 3000 rpm for 10 min. The upper phase was taken 2.5 mL and then added with another 2.5 mL of a distilled water, followed by adding 0.5 mL of $FeCl_3$ 0.1% w/v. The absorbance was then measured at 700 nm using UV spectrophotometer.

T47D cell assays

Cytotoxicity assay: The cytotoxicity assay of the fraction against T47D breast cancer cell was carried out using (3-(4,5-dimethylthiazol-2-yl)-2,5-diphenyltetrazolium bromide (MTT) method²⁷. The T47D cell was cultured on the RPMI media, whereas the normal cell (Vero) was cultured on the M199 media. Each of them contained FBS 10%, penicillin-streptomycin 1% and fungizone 0.5%. A series of working solution was prepared with concentrations as followed: 7.81, 15.62, 31.25, 62.5, 125, 250 and 500 μ g mL^{-1} , meanwhile cisplatin (15 μ M) was used as the positive control. The cell viability was determined at 595 nm and the absorbance was converted into the percentage viability using a plate reader. The IC_{50} was calculated by plotting the percentage viability against the concentration of the fraction. Subsequently, the Selectivity Index (SI) was defined according to the ratio between the IC_{50} of vero cell and the IC_{50} of T47D cell.

Apoptotic observation: Thousand microliters of 5×10^5 cells/well was seeded into 6-well plate and then incubated for a week. Two separate cells were treated with 900 μ L of the diethyl ether fraction and cisplatin, respectively with the selected concentrations based on the cytotoxicity assay. For the negative control, the same volume of a cultured medium was added and then incubated for 24 h. The medium was then transferred into a conical, washed using 500 μ L of PBS and harvested by adding 200 μ L of trypsin-EDTA 0.25%. This was followed by incubation for 3 min to let the cell detached from the bottom of the plate. The culture medium 1000 μ L mL^{-1} was added while re-suspending the cells to be transferred to the same conical. The cells were then centrifuged (2000 rpm, 5 min) and the media were discarded. The precipitated cells were collected and then dissolved in annexin V-FLOUS kit buffer followed by adding 2 μ L of PI and 2 μ L of annexin V. The cells suspension was then homogenized over 10 min at a room temperature and transferred to the flow cytometric tube for apoptotic observation.

Cell cycle observation: The same procedure with the previous apoptotic assay preparation was applied, but a little bit difference was made after washing the precipitated cells using a cold PBS. The cells were then added with flow cytometric reagent composed of 25 μ L of PI, 1 μ L of RNase and 0.5 μ L of triton-X. The mixture was then topped up to 500 μ L using PBS for each sample. The cells suspension was re-homogenized and then transferred into the flow cytometric tube. The sample was then analyzed using flow cytometer to determine

the cell cycle profile. The flow cytometric data was analyzed using flowing program to visualize the cells distribution at each phase of the cells cycle.

Structural identification of the most active fraction: The structural identification of the most active fraction was carried on GC-MS. For this 1 mg of fraction was dissolved in 1 mL of dichloromethane. The Rtx[®]-50 column (30×250×0.25 μm) was used as the stationary phase with helium as a carrier gas at a flow rate of 1 mL min⁻¹ and a pressure of 8.80 psi. The GC oven temperature was kept at 70°C and 300°C for initial and final temperature, respectively. The temperature rate increase was set at 10°C min⁻¹ during 15 min. Splitless injections were implemented with liquid injection method in this experiment. A library search for the structural identification was carried out using Wiley 7 Nist05 library (<http://www.sisweb.com/software/ms/wiley.htm>).

Molecular docking: The *in silico* prediction of chemical substances which were identified in GC-MS for the most active fraction carried out by docking the compounds into 10 representative protein targets from the selected bacteria and T47D cells, respectively. The ligands were sketched and geometrically minimized using ACD Chems sketch (www.acdlabs.com) and Marvin Sketch (www.chemaxon.com), respectively. The ligands and proteins were then prepared using AutoDockTools 1.5.6 (www.autodock.scripps.edu). The proteins were added with polar hydrogen and given by Kollman charge, whereas the ligands were given by Gasteiger charges. The grid was centered on each protein binding site and the docking was then performed using AutoDock Vina embedded in PyRx version 8.0 (www.autodock.scripps.edu).

The hit of protein was selected based on the lowest mean of free energy of binding (ΔG_{bind}), whereas a combination of a low ΔG_{bind} and hydrogen bond (H-bond) interaction was considered to select the hit of ligand. The selected docking pose was visualized using discovery studio 3.5 (www.accelrys.com).

RESULTS AND DISCUSSION

Fungal endophyte culture: A fungal endophyte namely *Trichaptum* sp. (Fig. 1a) which was isolated from *Phyllanthus niruri* leaves, physically characterized as a white fungal colony (Fig. 1b). The fungal morphology was identified by Mycology Laboratory, Agriculture Faculty (Gadjah Mada University, Indonesia) 45, stated that the sample had characteristics as followed: A helix solid mycelium, composed of dark hyphae pigmen and having uniform sclerotia. For instance, these characteristics were microscopically equal to the genus of *Trichaptum* sp., as described by the literature²⁸. The ethyl acetate extract of the fungal endophyte was collected in a considerably high yield (40%), therefore this is potential to be a good source of producing bioactive compounds.

Fungal molecular ecology needed the biggest sequence of DNA region to have a universal barcode sequence. The ITS gene for fungi was an important tool to precisely identify the molecular systematic of the tested fungal sample at genus and even species levels. The BLAST analysis of rDNA gene sequences of ITS demonstrated the highest similarity with *Trichaptum* sp., with percentage of homology was 99% towards a unique identifier utilizing *Trichaptum* sp. E7082 from the repository. Hence, based on the molecular

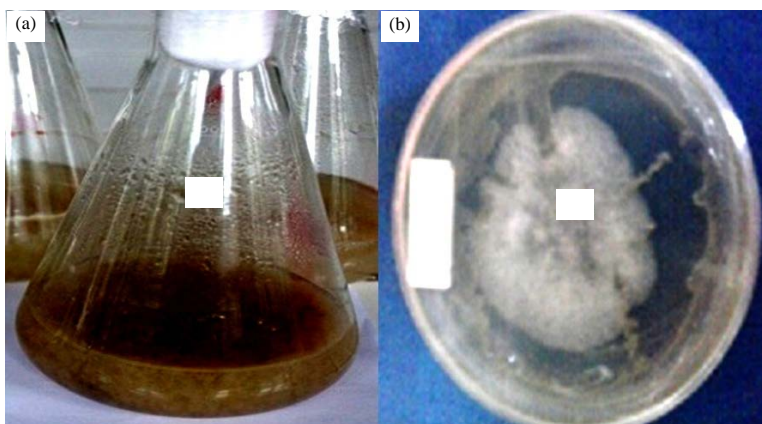


Fig. 1(a-b): (a) Fungal culture of *Trichaptum* sp., in 14th day of incubation and (b) The morphology of *Trichaptum* sp., with 7 days in age

Table 1: Sequence of ITS rDNA isolate (coded as BJ) and the BLAST result of the most similar taxon

ITS_4 Reverse

ATTGTCAAAGTATTTGTCTCGAGAGAGACGGCTAGAAGCGTGAATCAATAAACTTCACCACCGCAGC
 CAGATAATTATCACACTGAAGGCGATCCGTAAGGTTCACTAATGCATTCAGAGGAGTCTGACTGGCGA
 AGCCGACACAGCCTCAAGTCCAAGCCCAAAATCTTACTAGAAAAATTCAGGGGTTGAGAATACCATGAGACTCAAACAGGCATACTCCTCGGAATACCAAGGAGTGCAG
 GTGCGTTCAAAGATTGATGATTCACACTGAATTCTGCAATTCACATTACTTATCGCATTTTCGCTGCGTTCATCGATGCGAGAGCCAAGAGATCCG
 TGCTGAAAGTTGATATATTGTGTTATACACAGTGTACATTTATAACTGAAGTGTGTTGGTAAAACGCAAGAGAAGGCTTGTCTGACTGACTTTTACAAGATCAGTTACACCGCTCT
 CTTACATGAAGTGCACAGAGGT
 AGAGTGGATGAGCCAGGCGTGCACATACCCCAAAAAGAGGTCAGCTACAACCTGTTCAAAAACGATAATGATCCTTCCGAGGTTACCTACGAAACCTTGTACGACTTTTACTC

ITS_5 Forward

TTATCGAGTTTTGAACAGGTTGTAGTGCACCTCTTTTTGGGGTATGTGCACGCTGGCTCATCCACTCTCAACCTCTGTGCATTCATGTAAGAGAGCGGTGTAAGCTGATCTTGTA
 AAAAGTCAGTGACAAGCCTTCTTTCGTTTTACCACAAACACTTCAGTTATAGAATGTACTGTGTATAACACAATATATAACAACCTTCAGCAACGGATCTCTGGCTCTCGCATC
 GATGAAGAACGCAGGAAATGCGATAAGTAATGTGAATTGCAGAATTCAGTGAATCATCGAATCTTGAACGCACCTTGACTCCTTGGTATTCCGAGGAGTATGCCTGTTGAGT
 CTCATGGTATTCTCAACCCCTGAATTTTTCTAGTAAAGATTTGGTGGGCTTGACTTGGAGGCTGTGTCGGCTCTCGCCAGTGCAGTCTCTGAAATGCATTAGTGTGAACCTTACG
 GATCGCCTTCAGTGTGATAATTATCTGCGCTGCGGTGGTGAAGTATTTAATGAATTCACGCTTCTAGCCGCTCTCTCGAGACAAATACTTTGACAATCTGAGCTCAATCAGGTAG
 GATTACCCGCTGAACCTAAGCATATCAATA

Contig-sample

TTATCGAGTTTTGAACAGGTTGTAGTGCACCTCTTTTTGGGGTATGTGCACGCTGGCTCATCCACTCTCAACCTCTGTGCATTCATGTAAGAGAGCGGTGTAAGCTGATCTTGTA
 AAAAGTCAGTGACAAGCCTTCTTTCGTTTTACCACAAACACTTCAGTTATAGAATGTACTGTGTATAACACAATATATAACAACCTTCAGCAACGGATCTCTGGCTCTCGCATC
 GATGAAGAACGCAGGAAATGCGATAAGTAATGTGAATTGCAGAATTCAGTGAATCATCGAATCTTGAACGCACCTTGACTCCTTGGTATTCCGAGGAGTATGCCTGTTGAGT
 CTCATGGTATTCTCAACCCCTGAATTTTTCTAGTAAAGATTTGGTGGGCTTGACTTGGAGGCTGTGTCGGCTCTCGCCAGTGCAGTCTCTGAAATGCATTAGTGTGAACCTTACG
 GATCGCCTTCAGTGTGATAATTATCTGCGCTGCGGTGGTGAAGTATTTAATGAATTCACGCTTCTAGCCGCTCTCTCGAGACAAATACTTTGACAAT

E7082: Coded for *Trichaptum* sp., a species used as the reference, AJ536658: The code to access in DDBJ or NCBI, *Trichaptum* sp., E7082 (Accession no: AJ536658), Homology: 99%, Max score: 1040, Total score: 1040, Query coverage: 100%, E-value: 0.0, Max identities: 566/567 (99%) and Gaps: 1/567 (0%)

Table 2: Results of the disc diffusion assay of the fractions against the bacteria

Fraction	Loading (μg)	Growth inhibition zone (mm)				
		<i>Staphylococcus aureus</i>	<i>Escherichia coli</i>	<i>Salmonella thypi</i>	Positive control	Negative control
n-hexane	62.5	ND	ND	ND	23	ND
	125	ND	ND	ND		
	250	ND	ND	ND		
	500	ND	ND	2		
	1000	5	7	3		
Diethyl ether	62.5	1	ND	3	20	ND
	125	4	4	5		
	250	5	5	5		
	500	7	9	7		
	1000	14	11	13		
Ethanol 96%	62.5	ND	ND	ND	17	ND
	125	ND	ND	ND		
	250	ND	ND	ND		
	500	ND	1	9		
	1000	2	4	11		

ND: Not detected

genetic analysis, the fungal endophyte was confirmed its genus as *Trichaptum* sp. The sequence of ITS rDNA isolate and the BLAST result of the most similar taxon were presented in Table 1.

Screening of active fraction: The preliminary determination of antibacterial activities of the fractions was necessary to select which fraction would be potential for further testing. Table 2 presented the inhibition zone of three fractions (n-hexane, diethyl ether and ethanol 96%) towards *S. aureus*, *E. coli* and *S. thypi*. As results, diethyl ether fraction demonstrated a higher inhibition towards the bacterial growth than other two fractions. In the lowest concentration

(62.5 $\mu\text{g mL}^{-1}$), diethyl ether fraction inhibited both *S. aureus* and *S. thypi*, whereas neither n-hexane nor ethanol 96% fractions performed any inhibition. The inhibition of all bacteria by diethyl ether fraction was observed at concentration 125 $\mu\text{g mL}^{-1}$, since then the inhibition was proportionally increased along with the higher concentration of the fraction. Towards this fraction, all bacteria are similarly susceptible as shown by its close values of the inhibition zone starting from 125-1000 $\mu\text{g mL}^{-1}$. On the other hand, n-hexane and ethanol 96% fractions were more likely susceptible towards *E. coli* and *S. thypi*, respectively as shown by its higher inhibitions at 1000 $\mu\text{g mL}^{-1}$. Although, they can strongly inhibit the bacteria at the highest

concentration only, however, it was decided to include them for further IC_{50} calculations due to its potential antimicrobial activities to more specific bacteria as discussed.

Minimum Inhibition Concentration (MIC) and IC_{50} calculation:

The potent fraction was justified from its capability to inhibit the bacteria at the minimum concentration. When the fraction was able to inhibit at least 50% of the bacterial growth, only the IC_{50} value would be defined. Table 3 presented the MIC and IC_{50} value of each fraction against three bacteria. According to the susceptibility, the diethyl ether was the best fraction due to its capability to inhibit all bacteria at a lower concentration than two other fractions. The diethyl ether fraction has less than $100 \mu\text{g mL}^{-1}$ of IC_{50} to all bacteria indicating its broad spectrum activity. The *E. coli* was the most susceptible bacteria towards the diethyl ether fraction as it showed the lowest IC_{50} value ($23.98 \mu\text{g mL}^{-1}$) among three bacteria. Either n-hexane or ethanol 96% was less sensitive than diethyl ether, as shown by its IC_{50} value with more than $100 \mu\text{g mL}^{-1}$. However, as indicated in the preliminary antibacterial assay, ethanol 96% fraction selectively inhibited *S. typhi* more than other bacteria due to its IC_{50} value i.e., $98.11 \mu\text{g mL}^{-1}$, which was potential for a narrow spectrum antibacterial. The least susceptible fraction was detected on n-hexane as it showed more than $100 \mu\text{g mL}^{-1}$ of IC_{50} to all bacteria.

Total phenolic content: The total phenolic content is associated with the reducing capacity of the compounds under redox reactions. Table 4 presented the total phenolic content of the three fractions which was found in a quite broad range. Having its polar character, phenolic compounds were more soluble in a polar solvent such as ethanol 96% than in semipolar (diethyl ether) and nonpolar (n-hexane) solvents. However, in the diethyl ether, the total phenolic content was quite high that might contribute in the bacterial inhibition as known that phenol could denature the protein leading to a bacterial eradication²⁹.

Antioxidant activity: Hydrogen peroxide is rapidly decomposed into oxygen and water. This may form hydroxyl radical able to modulate the lipid peroxidation process lead to the cell damage. In this assay, all fractions possessed the free radical scavenging activity at 34-85% (Fig. 2a). Among all fractions, ethanol 95% demonstrated the highest radical scavenging (85%) which was almost comparable with vitamin C (95%) as the positive control. This was in agreement with the reducing power capacity assay (Fig. 2b) which demonstrated the same order for all three fractions. The ethanol 96%

fraction was able to reduce the reduction of Fe (III) to Fe (II) in such a way that those compounds donated electron to stabilize the radicals up to 80% in the ethanol, which was almost comparable to that vitamin C (90%). These two antioxidant activities corresponded to the total phenolic content, in which ethanol as a polar solvent able to strongly

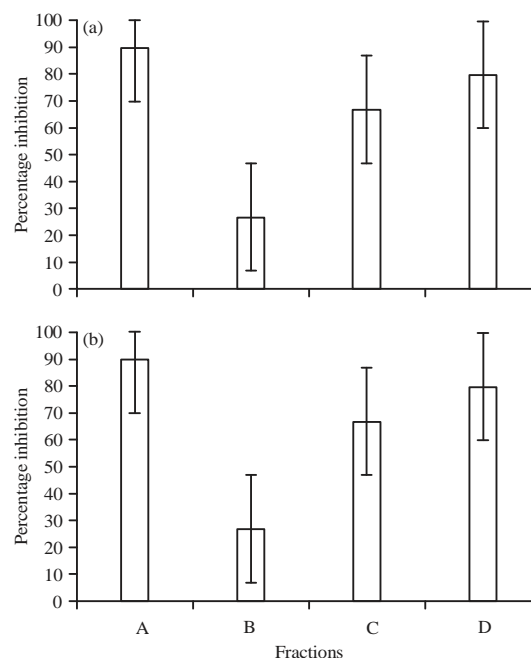


Fig. 2(a-b): Antioxidant activity of three fractions using methods, (a) H_2O_2 free radical scavenging and (b) Reducing power capacity, A: Vitamin C, B: n-hexane fraction, C: Diethyl ether fraction and D: Ethanol 96% fraction. The graph was prepared using Microsoft Excel 2010 (www.microsoft.com)

Table 3: IC_{50} and MIC value of three fractions against *Staphylococcus aureus*, *Escherichia coli* and *Salmonella typhi*

Bacteria	Samples					
	n-hexane		Diethyl ether		Ethanol 96%	
	IC_{50}	MIC	IC_{50}	MIC	IC_{50}	MIC
<i>E. coli</i>	111.23	>500	23.98	125	102.34	>500
<i>S. aureus</i>	245.76	>500	60.14	250	107.98	>500
<i>S. typhi</i>	113.09	>500	45.11	125	98.11	>500

Table 4: Total phenolic content of three fractions

Fraction	Total phenolic content (mg GAE g^{-1} fraction)
n-hexane	13.14 ± 0.43
Diethyl ether	56.98 ± 0.11
Ethanol 96%	65.70 ± 0.87

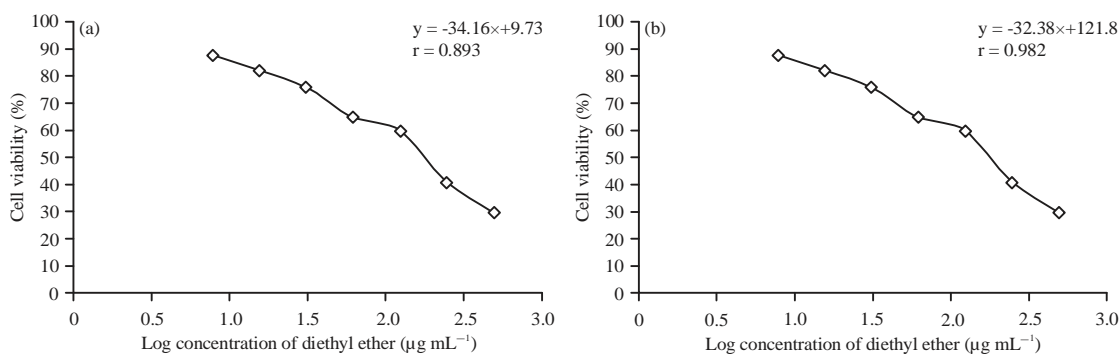


Fig. 3(a-b): Drug-dose response curve of diethyl ether fraction against the percentage viability of (a) T47D and (b) Vero cell with $p < 0.05$. The graph was prepared using Microsoft Excel 2010 (www.microsoft.com)

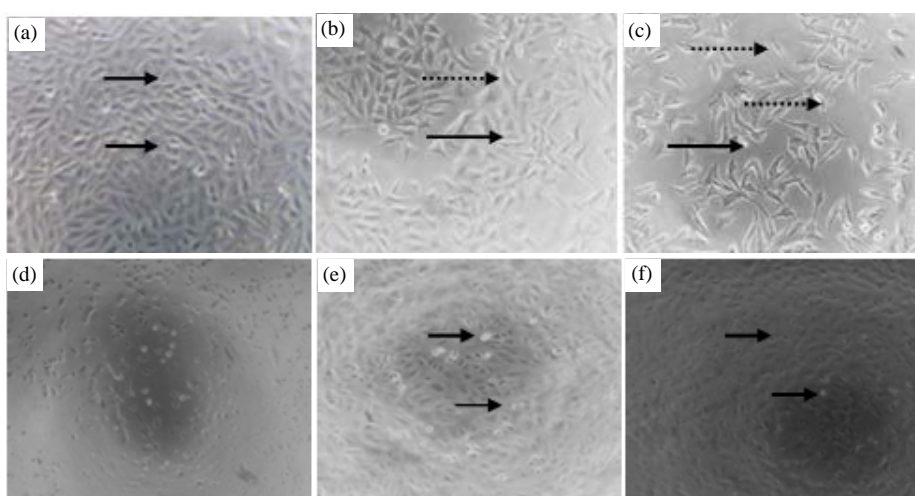


Fig. 4(a-f): Effect of diethyl ether fraction towards T47D⁷³ and vero cells (d-f). The viewing was performed under inverted microscope with 100x of magnitudes, (a) Negative control (b) Diethyl ether fraction 5 $\mu\text{g mL}^{-1}$, (c) 10 $\mu\text{g mL}^{-1}$, (d) Negative control, (e) Diethyl ether fraction 250 $\mu\text{g mL}^{-1}$ and (f) Diethyl ether fraction 500 $\mu\text{g mL}^{-1}$. The arrow indicated the living cell whereas the dashed arrow indicated the morphological alteration

Table 5: Results of cytotoxicity assay against T47D cell line

Fractions	IC ₅₀ T47D ($\mu\text{g mL}^{-1}$)	IC ₅₀ vero ($\mu\text{g mL}^{-1}$)	Selectivity Index (SI)
n-hexane	92.64 ± 0.76	245.98 ± 1.65	2.66
Diethyl ether	13.07 ± 0.23	230.87 ± 0.96	17.66
Ethanol 96%	67.56 ± 2.34	339.32 ± 1.65	5.02

fractionate phenolic based compounds. This antioxidant activity could be associated with a lipid peroxidation inhibition.

T47D cell assay

Cytotoxicity assay: The T47D is breast cancer cell lines, which is primarily used as the model in a breast cancer research³⁰. The inhibition of this cell up to 50% was associated with the potential anticancer from the fractions (Table 5). All fractions were observed having IC₅₀ less than 100 $\mu\text{g mL}^{-1}$ indicating

its potential as an anticancer with diethyl ether fraction re-showing the lowest IC₅₀ value than two others. Fortunately, this fraction showed the highest Selectivity Index (SI) indicating its selectivity was rather to cancer than the normal cells. There have been an agreement between antibacterial and cytotoxicity assays, hence, this fraction was promiscuous for chemotherapeutics against both bacteria and cancer cells. Figure 3a and b plotted the concentration of diethyl ether fraction against the percentage inhibition of T47D cell line and vero cell, respectively.

The morphology of T47D upon diethyl ether exposure was observed altering the cell being shrunk, died and reduced in the cell number. These effects were verified by comparing them with the negative control, in which the cell without treatment had no morphologic alteration (Fig. 4a-c). The

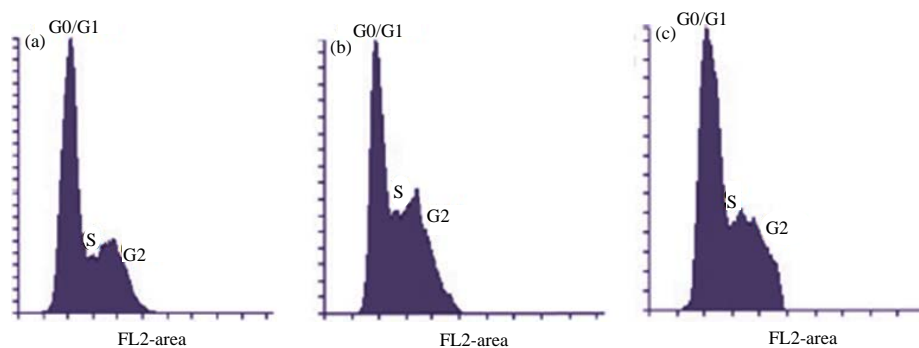


Fig. 5(a-c): Flow cytometry detection of cells cycle distribution, (a) Negative control, (b) Cisplatin and (c) Diethyl ether fraction treatment. In 6-well plate, 5×10^5 cells was cultured and incubated for 24 h in high glucose DMEM either with or without treatments. The detection of flow cytometri was done using PI reagent towards T47D cell after $4 \mu\text{g mL}^{-1}$ of diethyl ether fraction dan $2.5 \mu\text{M}$ of cisplatin exposure or the combination of its all three components, G0 is a phase that cell preparing to enter the G1 cell cycle

Table 6: Percentage of cells cycle distribution after diethyl ether and cisplatin exposure towards T47D cell

Samples	G1 phase (%)	S phase (%)	G2/M phase (%)	CV (%)	G1 phase (%)
Negative control	48.65	11.87	24.75	8.87	48.65
Cisplatin	41.86	13.12	27.54	9.45	41.86
Diethyl ether fraction	25.87	27.43	17.40	6.87	25.87

cytotoxic effect of diethyl ether fraction towards vero cells based on IC_{50} value as well as the morphology profile, showed a milder effect than T47D cells. However, the diethyl ether fraction exposure altered the morphology of the Vero cell to be shrinking, circling and detaching from the bottom of the well although it needed more concentrations to give the same effect with that of T47D (Fig. 4d-f).

Modulation of T47D cell cycle: As occurred in normal cells, the DNA synthesis in cancer ones also went through the cells cycle. One of the main targets in blocking the cancer cells proliferation was done by modulating the cells cycle, which could be observed using flow cytometric method. Flow cytometry was able to detect every single phase in the cells cycle based on chromosome numbers for each phase (G1, S and G2/M). The G1 phase had $2n$ (diploid) chromosome, whereas S phase replicated them as the preparation to enter G2 phase. The number of chromosome sets in this stage was between $2n$ and $4n$, meanwhile G2 phase formed $4n$ (two diploid cell) chromosome³¹. The flow cytometric analysis using flowing program was presented in Fig. 5 and its detail cells cycle percentage could be seen in Table 6.

The negative control was distributed over G1, S and G2/M phases. The result showed that cisplatin caused the cell accumulation at the S phase. Likewise, diethyl ether fraction

caused the cell accumulation at the S phase compared to the negative control. In the treatment of diethyl ether fraction, the percentage of cells cycle distribution at the S phase was observed as 27.43%, which even higher than a single cisplatin, noted as 13.12%. It was found an increment on cells accumulation at the S phase for diethyl ether fraction compared to that negative control as nominally observed from 11.87-27.43%. This might happen because of cell cycle arrest at that stage.

The treatment of diethyl ether fraction at the lowest concentration did not cause cell death and even badly increased the cell population at the S phase. It was known that the cell cycle progress was activated sequentially from cyclin or CDK complex which was specific in each cell cycle phase. In both G1 dan S phases, the cell regulation was inhibited by cyclin-dependent kinase inhibitor (CKI) such as protein of INK4 and CIP/KIP along with tumor suppressor genes, including pRB and p53. In this study, the mutated T47D at p53 was utilized, so that the anticancer mechanism of diethyl ether fraction could posses via p53 independent pathway.

The independent pathway from p53 status and S arrest case might happen because a rapid decline of Cdc25A phosphatase activity, which was impacted by the ubiquitination along with its degradation by proteosome. This decline failed to activate CDK2 kinase by inhibiting its dephosphorilation at Thr14 and Tyr15. The phosphorilation of Cdc25A was mediated by ATM/ATR-Chk2/Chk1 cascade pathway^{32,33}. The degradation of Cdc25A phosphatase was dependent to ATM-Chk2. This ATM-Chk2 inhibited CDK2, which shall initiate Cdc45 (replication checkpoint) leading to a DNA replication speed reduction. This then stopped the DNA replication and triggered the S arrest³⁴.

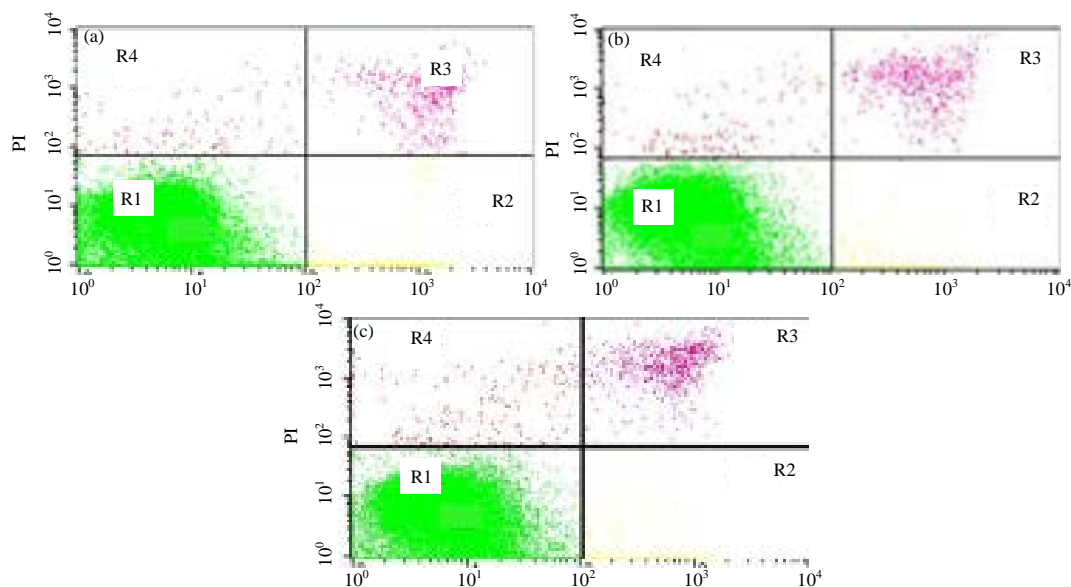


Fig. 6(a-c): Effect of apoptotic induction after diethyl ether and cisplatin treatment, (a) Negative control, (b) Cisplatin and (c) Diethyl ether fraction treatment. Cells were cultured with 5×10^5 density in 6-well plate and incubated for 24 h in high glucose DMEM with and without treatment, R1, R2, R3 and R4 quadrant located the survived cell, initial apoptosis, final apoptosis and necrosis, respectively

Table 7: Percentage of cell death after diethyl ether and cisplatin exposure towards T47D cell

Parameters	Negative control (%)	Diethyl ether fraction ($4 \mu\text{g mL}^{-1}$) (%)	Cisplatin ($2.5 \mu\text{M}$) (%)
Initial apoptosis (%)	1.43	8.89	2.65
Final apoptosis (%)	1.09	1.34	2.98
Necrosis (%)	0.87	1.65	1.02
Total	3.39	11.88	6.65

The p38MPK pathway also took the role in the cell cycle inhibition at the S phase, which could be going through p53-independence. Protein p38 could directly phosphorylate and stabilize an *in vivo* p21³⁵. Likewise, p38 protein also could phosphorylate and promote the degradation of Cdc25A which contributed in stopping the cell cycle at the S phase³⁶.

In the p53 mutated tumor cell, it was known about the response reduction towards agents which induced apoptosis, thus, could serve as the antineoplastic agent working on a resistant DNA damage. This mutation will cause a failure of a chemotherapeutic agent such as doxorubicin in activating p53 via DNA intercalation as well as its interaction with topoisomerase IIa. The T47D cell could be resistant towards doxorubicin due to the mutated p53 gen^{37,38}. This opened the chance of the diethyl ether fraction at a lower dose could be developed as a co-chemotherapeutic agent.

The anticancer activity of the diethyl ether fraction serving as a cell arrest inductive agent at the S phase could be developed by introducing it with an arrest damaging agent.

When the p53 deficient cancer cell was introduced by the DNA damaging agent in combination with a checkpoint ruining agent at the S phase, the cell would be triggered to enter the mitosis phase while carrying the damage DNA ending to an apoptosis and cell deaths (a mitotic catastrophe).

The mechanism via this checkpoint impairment was believed as one of the strategies to selectively kill the cancer cells. These cells were suffering defect on p53 gen but at the same time, the normal cells were still protected having wild type p53 gen³⁹⁻⁴¹. A few compounds have been reported as the S checkpoint abrogator such as AZD7762 worked by inhibiting phosphorylation of Cdc25A. This phosphorylation was done by Chk1 and Chk2 using gemcitabine as the S arrest inductor⁴².

Apoptosis of T47D cell: The cells death being caused by apoptosis or necrosis could be differentiated using Propidium Iodide (PI) coloring agent via a DNA intercalation⁴³ (Fig. 6). The apoptotic induction resulted a percentage of cell death, which was affected by the treatments of either diethyl ether fraction or cisplatin presented in Table 7.

The result showed that without any treatment, the T47D cell could be survive up to 96.61% of living cells and it was only 3.39% of cell deaths being observed. The treatment using diethyl ether fraction was found to increase the T47D cell deaths percentage up to 11.88%, even better than cisplatin

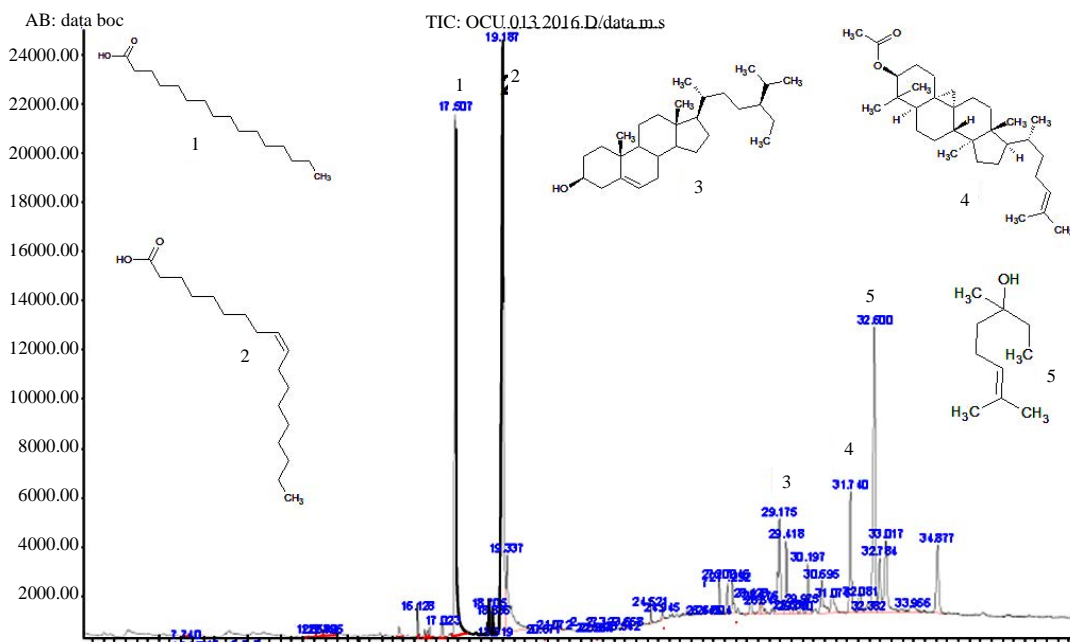


Fig. 7: GC chromatogram of diethyl ether fraction of the fungal endophyte

which could kill the cells up to 6.65% only. This suggested that the diethyl ether fraction could be more potent than that of positive control.

The T47D was a breast cancer cell having caspase-3 wild type, caspase-7 wild type, ER/PR positive and p53 mutant⁴⁴. Cisplatin was reported able to induce Bcl-2 downregulation on the T47D breast cancer cell⁴⁵ and also to form a DNA crosslink causing DNA damages leading to apoptosis⁴⁶. The Bcl-2 downregulation (antiapoptotic protein) would decrease the cell defense, therefore it increased the susceptibility towards chemotherapeutic agent⁴⁷. The diethyl ether fraction was found to increase apoptosis and undergo the cell cycle modulation at the S phase. This caused the cell being failed to replicate and stop the proliferation. However, there might happen intermolecular antagonisms among compounds in the diethyl ether fraction, therefore, further study was necessary to investigate the individual apoptotic induction for each compounds identified in the fraction. Moreover, it is well studied that the apoptosis could be induced via NF- κ B inhibition, a protein complex that controls transcription of DNA, cytokine production and cell survival. The proteins such as p53 mutant, Bcl-2 and NF- κ B which could be involved in such molecular mechanism should be more specifically discussed.

Structural identification of the most active fraction: The fast structural identification of compounds in diethyl ether as the most active fraction using GC-MS, revealed five compounds at

different retention times (R_t) with higher peak intensities than others in the GC chromatogram (Fig. 7). These compounds were identified based on their MS profile including the matched molecular weight as well as its fragmentation with compounds database in Wiley 7 Nist05 library. Five compounds with molecular weight (m/z) 256 (15%), 282 (22%), 414 (4.5%), 468 (4%) and 156 (12%) were identified as hexadecanoic acid (1; R_t 17.507 min), 9-octadecanoic acid (Z) (2; R_t 19.187 min), gamma sitosterol (3; R_t 29.175 min), 9,19-cyclolanost-24-en-3-ol acetate (4; R_t 31.740 min) and dihydrolinalool (5; R_t 32.597 min), respectively. Instead of GC only detected compounds in high intensities for the volatile ones which usually have more hydrophobic characters, another 9 compounds with very low intensities (<1%) were also observed (Table S1). These compounds were characterized having more drug-like structures according to the Lipinski rule of five⁴⁸ than the previous ones. These compounds might be low detected in GC because they were less volatile due to the presence of hydrophylic functional groups. In contrast, they could highly present if other identification method such as LC-MS were used. Therefore, we included them in the list of compounds for further study on *in silico* protein-ligand interactions.

Molecular docking

***In silico* activity against protein targets in *E. coli*:** There have been more than 4,000 Open Reading Frames (ORFs) characterized in the *E. coli* genome, encodes approximately

Table S1: Compounds have been identified from diethyl ether fraction of the fungal endophyte

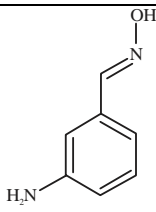
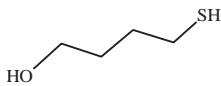
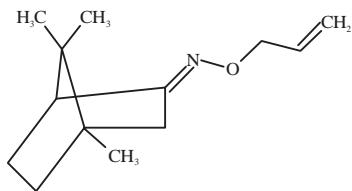
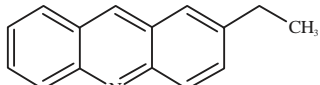
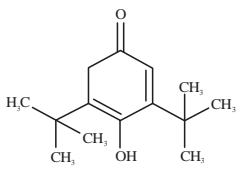
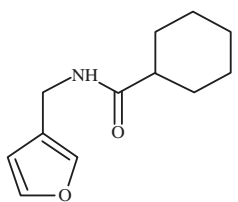
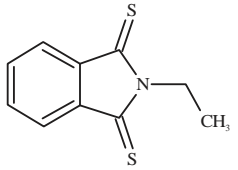
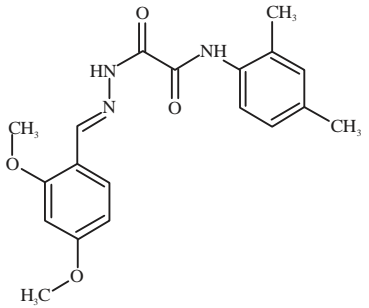
Codes	R _t (Min)	Molecular weight	Names (Molecular weight)	Structures
6	12.548	136	m-aminobenzaldehyde oxime	
7	12.806	106	4-sulfanyl-1-butanol	
8	23.554	207	4,7,7-trimethylbicyclo[2.2.1]heptan-2-one O-allyloxime	
9	26.443	207	2-ethylacridine	
10	26.807	222	2,4-cyclohexadien-1-one, 3,5-bis [1,1-dimethylethyl]-4-hydroxy	
11	27.293	207	Cyclohexanecarboxamide, N-furfuryl	
12	28.545	207	N-ethyl-1,3-dithioisindoline	
13	31.080	355	2',4'-dimethyloxanic acid N'-veratrylidenehydrazide	

Table S1: (Supplementary data continued)

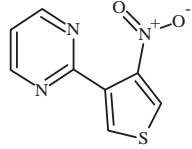
Codes	R _t (Min)	Molecular weight	Names (Molecular weight)	Structures
14	32.081	207	2-[4'-dinitro-3'-thienyl]pyrimidine	

Table 8: $\Delta G_{\text{binding}}$ of 14 ligands were docked into 10 proteins in *Escherichia coli*

Ligands	ΔG_{bind} (kcal mol ⁻¹)									
	1152	1JYV	1MOS	1SZS	4DUH	1I30	1JZQ	1IX6	1OHA	2PTH
1	-4.6	-6.5	-5.6	-5.3	-5.9	-5.3	-5.3	-4.5	-5.0	-5.1
2	-4.9	-6.9	-4.6	-6.4	-6.6	-5.4	-5.4	-5.1	-5.8	-4.7
3	-6.4	-9.6	-8.0	-7.7	-6.3	-7.9	-7.7	-7.1	-7.7	-5.5
4	-6.8	-10.7	-6.7	-8.5	-5.5	-8.7	-9.3	-8.0	-8.3	-5.1
5	-5.2	-6.6	-4.8	-5.8	-5.4	-5.2	-5.6	-4.9	-5.0	-4.9
6	-5.3	-6.0	-5.6	-6.5	-6.1	-5.9	-5.4	-6.0	-6.2	-5.1
7	-3.2	-3.5	-3.5	-4.0	-3.7	-3.3	-3.3	-3.4	-3.5	-3.1
8	-6.2	-7.3	-5.9	-6.8	-5.3	-5.9	-6.5	-5.5	-5.6	-5.4
9	-6.5	-8.9	-7.1	-8.4	-8.3	-8.7	-8.4	-8.4	-6.8	-6.5
10	-6.3	-8.1	-6.1	-6.6	-6.3	-6.0	-6.8	-5.5	-6.3	-5.1
11	-6.0	-7.6	-6.6	-7.5	-7.0	-6.9	-6.5	-6.9	-6.2	-6.3
12	-5.2	-7.4	-4.7	-6.2	-5.7	-6.4	-5.8	-6.4	-5.5	-5.0
13	-6.9	-10.0	-7.6	-7.6	-8.2	-7.6	-8.8	-7.7	-8.5	-7.0
14	-6.0	-6.7	-6.3	-6.4	-6.5	-6.2	-6.3	-6.3	-6.3	-6.3
Mean	-5.7	-7.6	-5.9	-6.7	-6.2	-6.4	-6.5	-6.1	-6.2	-5.4

Table 9: Amino acid residues identified from the interaction of 14 ligands with 1JYV

Ligands	Amino acid residues	Ligands	Amino acid residues
Control	Lys15, Arg66, Tyr155, Asp65, Glu153, Asp14, Glu111	8	No H-bond
1	No H-bond	9	No H-bond
2	Arg66, Arg345	10	Trp62
3	No H-bond	11	Arg66
4	Lys42	12	No H-bond
5	Asp65	13	Glu44, Arg66, Arg345
6	Glu111, Tyr155	14	Lys15
7	Trp62, Arg66		

70% of protein remains in cytoplasm⁴⁹. Ten of them were used as the representative target to study the molecular mechanism of 14 ligands of the diethyl ether fraction. The proteins being used as the target in *E. coli* were methylerythritol phosphate cytidyltransferase (PDB 1152)⁵⁰, maltose binding periplasmic protein (MBP; PDB 1JYV)⁵¹, glutamine-fructose-6-phosphate aminotransferase (PDB 1MOS)⁵², -aminobutyrate aminotransferase (PDB 1SZS)⁵³, DNA gyrase (PDB 4DUH)⁵⁴, enoyl reductase (PDB 1I30)⁵⁵, isoleucyl tRNA synthetase (PDB 1JZQ)⁵⁶, aspartate aminotransferase (PDB 1IX6)⁵⁷, acetylglutamate kinase (PDB 1OHA)⁵⁸ and peptidyl tRNA hydroxylase (PDB 2PTH)⁵⁹. Table 8 presented the docking results of 14 ligands identified in diethyl ether fraction against diverse protein targets in *E. coli*.

As results, the ligands showed ΔG_{bind} at range -10.7 to -3.1 kcal mol⁻¹. According to the mean of the ΔG_{bind} , the lowest ΔG_{bind} went to the interaction between Maltose Binding Periplasmic (MBP) protein and the ligands, indicated its strongest binding interaction among 10 protein targets. Maltose binding periplasmic was a huge bacterial periplasmic protein (370 amino acid residues) involved in active transport and chemotaxis towards maltose. This enzyme worked under substantial conformational changes to let maltose binds to the ATP-binding cassette (ABC)-7 transporter, initiating downstream signaling for either transport or chemotaxis⁶⁰. Therefore, the MBP could be the selected protein target for further study. Table 9 presented the amino acid residues involved in the binding of 14 ligands.

From these 14 ligands, 10 of them were characterized having hydrogen bond interaction with MBP, whereas the remained four ligands were absent. The absent hydrogen bond interaction might be due to incorrect pose of the polar functional groups to interact with the nearest important amino acid residues. Therefore, the ΔG_{bind} of those compounds were significantly contributed by hydrophobic and other Van der Waals interactions. It was well studied that the strength of Van der Waals interaction was weaker than hydrogen bond interaction due to their distance bonds, i.e., >2.2 and 1.5-2.2 Å, respectively⁶¹.

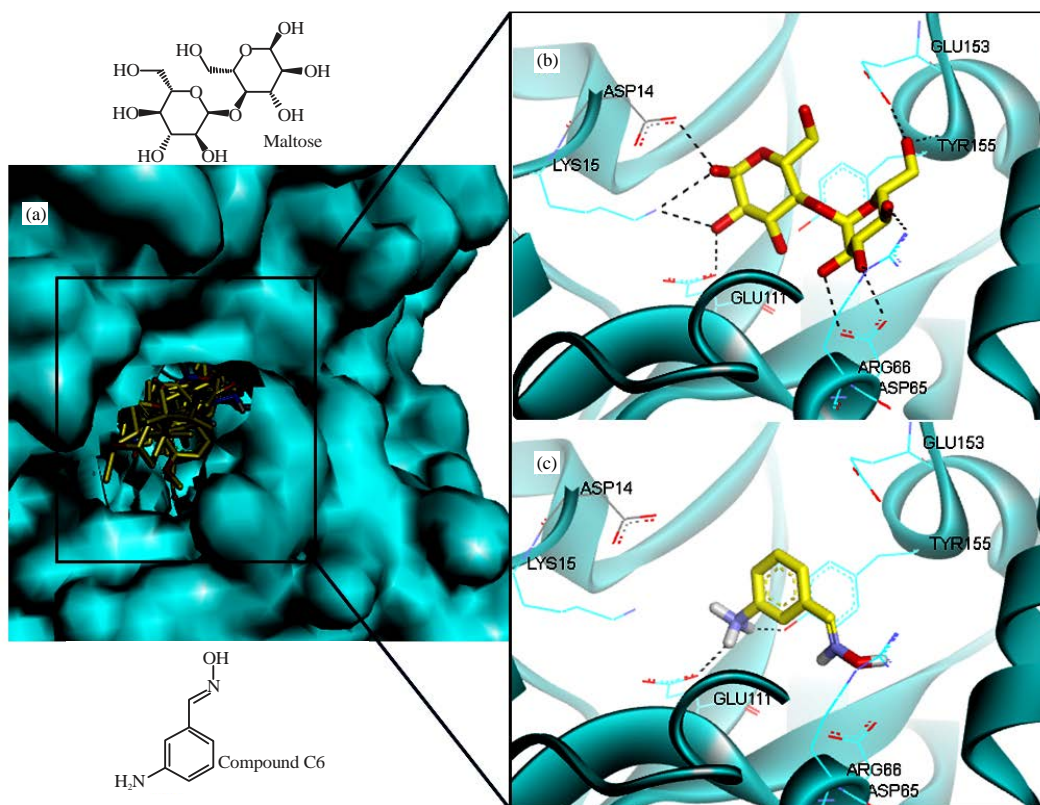


Fig. 8(a-c): (a) Superposition of 14 ligands in *Trichaptum* sp., meanwhile inset was the pose of (b) Maltose and (c) Compound 6 at the at the binding site of 1JVY. The individual poses of maltose and compound 6 was visualized as stick forms with carbon in yellow and standard colors of O and H. The superposition was presented in a surface protein, whereas the individual maltose and compound 6 was performed in ribbon. The picture was visualized using discovery studio 3.5 (www.accelrys.com)

Among 10 ligands that interacted with MBP via hydrogen bond interaction, six of them demonstrated binding modes similar to that of control ligand (maltose) indicating their potential to be developed as novel MBP inhibitors. The residues being identified in their binding modes were Lys15, Asp65, Arg66, Glu111 and Tyr155. Most of them had one interaction only with the residues, which was also a part of the positive control's binding mode. However, compound 6 (m-aminobenzaldehyde oxime) was identified possessing two hydrogen bond interactions with same residues of the positive control associating its more potential ligands to be optimized as MBP inhibitors. Figure 8 illustrated the superposition of 14 ligands at the binding site of MBP, positive control and the selected hit ligand-MBP molecular interaction. As visualized in Fig. 8c, compound 6 showed the similar binding mode towards MBP, i.e., hydrogen bond interaction with Glu111 and Tyr155. Although there were some interactions being missed, this compound could be a good lead model for further MBP inhibitor associating with its potency as antibacterial against *E. coli*.

***In silico* activity against protein targets in T47D cell:**

Likewise, the 14 same ligands were studied in the screening of 10 protein targets in the T47D. The protein targets were mainly concerned on human p53 with hot spot mutation R273C (PDB 4IBU)⁶² and pro-survival Bcl-2 (PDB 4B4S)⁶³ and NF- κ B inducing kinase (PDB 4DN5)⁶⁴ as suggested by previous T47D apoptotic studies. However, it was tried to seek for other possibilities in other protein targets which were expressed in the T47D. They were: C-src tyrosine kinase (PDB 3G5D)⁶⁵, human tubulin colchicine receptor (PDB 1SAO)⁶⁶, estrogen receptor DNA binding protein (PDB 1GWQ)⁶⁷, human oxidosqualene cyclase (PDB 1W6K)⁶⁸, ER α nuclear receptor (PDB 3ERT)⁶⁹, p38a MAP kinase (PDB 3HEG)⁷⁰ and Bcl-11 (PDB 1YS1)⁷¹. Table 10 presented the docking results of 14 ligands against diverse protein targets in T47D.

Likewise, the range of ΔG_{bind} for ligands against 10 protein targets in T47D was at -11.6 to -1.3 kcal mol⁻¹. Among three proteins which were suggested by T47D apoptotic studies, p53 mutant and NF- κ B had a lower ΔG_{bind} than Bcl-2. This

impressed that two of possible mechanisms on how diethyl ether fractions modulated the T47D apoptosis could be via p53 and/or NF- κ B inhibition. However, the evaluation on docking results was not obviously based on the ΔG_{bind} since frequently, the lower docking score was majorly contributed by Van der Waals interaction as mentioned before. The p53 mutant with PDB 4IBU was a human p53 mutant with hot spot R273C in complex with zinc ion, ethylene glycol and acetate ion, meanwhile NF- κ B with PDB 4DN5 was a human NF- κ B kinase in complex with phosphothiophosphoric-acid adenilate ester. Based on the structure of both crystallized ligands, the compounds identified in diethyl ether fraction seemed like no similar pharmacophoric features with them. The probability of compounds bound to the allosteric site of enzyme was there, but here, it was firstly focused on the active site. Hence, it was tried to seek for other protein which had a crystallized ligand mimicking the compounds presenting in the diethyl ether fraction.

Apparently, human oxydosqualene cyclase (PDB 1W6K) was identified having the lowest value in the mean of ΔG_{bind} among all 14 ligands. Again, this indicated its potential to be the protein target in blocking T47D cell growth. Human

oxydosqualene cyclase (OSC) is a membrane-bound enzyme, which catalyzes the formation of lanosterol, a precursor to synthesize human cholesterol⁷². Human cholesterol from lanosterol is a sterol isomerase, known to be modulated by several well known sterol biosynthesis inhibitor such as tamoxifen, a chemotherapeutic agent for breast cancer. Table 11 presented the amino acid residues involved in the binding of 14 ligands-OSC.

The control ligand (lanosterol) only showed one hydrogen bond interaction with Asp455. The major contributor in this ligand-protein interaction was hydrophobic character of steroid scaffold surrounded by non-polar amino acid residues such as Phe444, Phe521, Ile524, Phe696 and Ile702. One ligand, i.e., compound 3 demonstrated a similar pose with the control ligand due to the interaction with Asp455 via hydrogen bonding. This was because they beared a same steroid-based scaffold. Therefore, this compound indicated its potency as the lead for further optimization as OSC inhibitor. Figure 9 illustrated the superposition of 14 ligands at the binding site of the human OSC and the most active ligand-OSC molecular interaction.

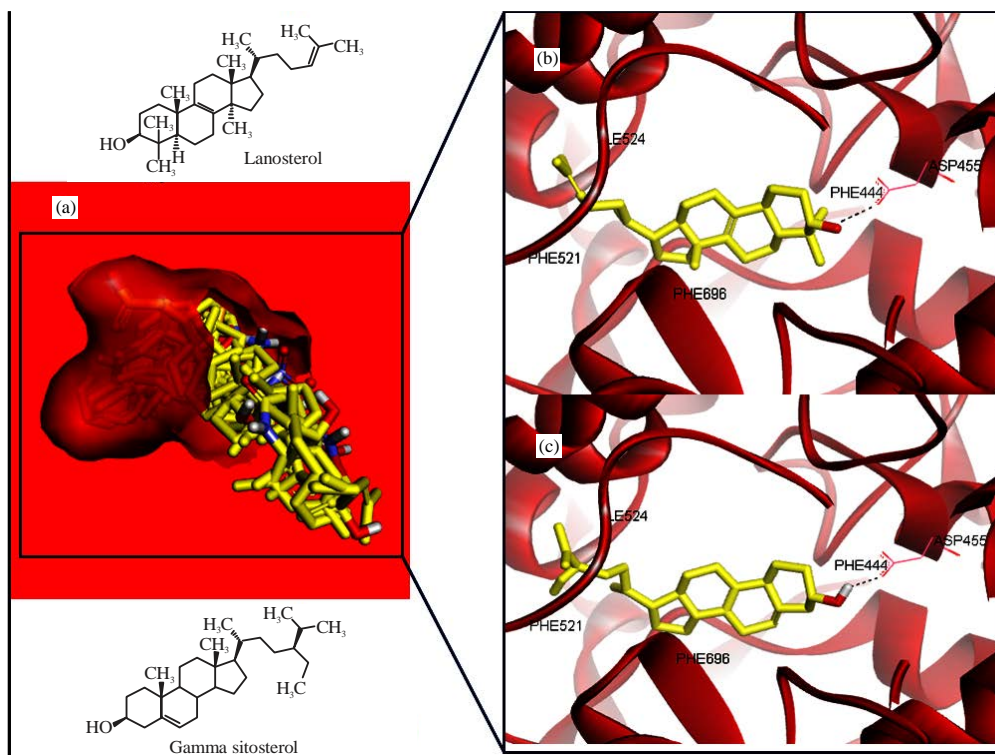


Fig. 9(a-c): (a) Superposition of 14 ligands in *Trichaptum* sp., meanwhile inset was the pose of (b) Lanosterol and (c) Compound 3 at the at the binding site of 1W6K. The individual poses of lanosterol and compound 3 was visualized as stick forms with carbon in yellow and standard colors of O and H. The superposition was presented in a surface protein, whereas the individual maltose and compound 6 was performed in ribbon. The picture was visualized using discovery studio 3.5 (www.accelrys.com)

Table 10: $\Delta G_{\text{binding}}$ of 14 ligands were docked into proteins in and T47D cell lines

Ligands	ΔG_{bind} (kcal mol ⁻¹)									
	1IBU	4B4S	4DN5	1SAO	3G5D	1GWQ	1W6K	3ERT	3HEG	1YS1
1	-4.4	-3.9	-5.6	-5.6	-5.6	-6.0	-7.0	-5.8	-5.7	-5.9
2	-4.6	-4.2	-5.9	-5.9	-5.8	-6.0	-7.7	-5.9	-6.3	-6.1
3	-6.9	-5.5	-8.9	-1.3	-7.7	-7.3	-11.6	-7.6	-7.5	-8.3
4	-5.8	-6.1	-6.5	-9.4	-8.3	-6.0	-10.6	-6.2	-7.2	-8.3
5	-4.1	-3.8	-5.5	-5.4	-5.5	-5.5	-6.2	-5.7	-5.3	-5.4
6	-5.5	-4.8	-6.0	-5.5	-5.5	-6.2	-6.4	-6.1	-5.7	-5.6
7	-3.5	-3.1	-3.3	-3.5	-3.1	-3.4	-3.7	-3.4	-3.3	-3.3
8	-5.5	-4.8	-6.2	-5.9	-6.6	-5.5	-7.5	-6.7	-6.0	-5.7
9	-5.5	-5.6	-8.8	-7.7	-8.4	-8.3	-10.3	-8.4	-7.2	-8.3
10	-5.0	-4.0	-6.6	-5.9	-7.0	-7.0	-8.5	-7.3	-6.8	-6.7
11	-5.2	-6.0	-7.2	-6.4	-6.9	-7.0	-8.3	-7.1	-6.3	-6.9
12	-4.0	-4.4	-6.7	-5.5	-6.2	-6.2	-7.4	-6.5	-6.2	-6.1
13	-6.7	-5.6	-8.7	-5.6	-5.6	-7.6	-10.7	-8.3	-7.3	-8.0
14	-5.4	-5.0	-6.4	-5.9	-5.8	-6.7	-7.3	-6.4	-5.7	-6.2
Mean	-5.15	-4.8	-6.6	-4.3	-6.3	-6.3	-8.1	-6.5	-6.2	-6.5

Table 11: Amino acid residues identified from the interaction of 14 ligands with 1W6K

Ligands	Amino acid residues	Ligands	Amino acid residues
Control	Asp455	8	Tyr704
1	His232, Ser339	9	No H-bond
2	His232, Ser339, Ile338	10	Tyr504, Tyr704
3	Asp455	11	His232
4	His232	12	No H-bond
5	No H-bond	13	Tyr98, Tyr503,
6	Gly380	14	Tyr98
7	No H-bond		

CONCLUSION

A fungal endophyte of *Trichaptum* sp., genus isolated from *Phyllanthus niruri* in organic fractions such as n-hexane, diethyl ether and ethanol 96% was studied in a various biological activities as antimicrobial, antioxidant and cytotoxic agent against breast cancer cell. Diethyl ether was selected as the most active fractions inhibiting the representative bacteria cell growth and T47D breast cancer cell lines, whereas ethanol 96% was found as the most active antioxidant. It was observed that *E. coli* was the most sensitive bacteria against the diethyl ether fraction. Further T47D cell assay revealed that the diethyl ether fraction served as cancer cytotoxic agent by modulating cell arrest as well as its apoptosis. The suggested proteins being involved in this molecular mechanism were p53, Bcl-2 and NF- κ B. In this study, we have a limitation in testing the activity of the fractions against *E. coli* and T47D breast cancer cell lines at enzyme or receptor level. This restricted more understanding of molecular mechanism on how fungal endophyte from *Phyllanthus niruri* served as antibacterial as well as anticancer. However, it was initiated to study the molecular mechanism of some representatives compounds identified in the diethyl ether fraction against diverse protein

targets in *E. coli* as well as T47D breast cancer cell lines. This was aimed to guide our further experiment in isolating compounds from the corresponding endophyte and testing them against the selected protein targets. The docking studies showed that compounds bearing benzaldehyde oxime were potential for maltose binding periplasmic associating with their potencies as an antibacterial agent. Beside, compounds bearing steroid is also potential for human OSC inhibitor due to its disclose scaffold with the control ligand of human OSC. Overall, the novelty of this study is the discovery of *Trichaptum* sp., in a fungal endophyte genus isolated and cultivated from *Phyllanthus niruri* which never been reported. Moreover, the organic fractions this endophyte is found active as antibacterial, antioxidant and T47D breast cancer cytotoxic agent. Further study would be emphasized on *in vitro* MBP and OSC inhibition assay by diethyl ether fraction to prove the concept of molecular docking.

ACKNOWLEDGMENTS

We gratefully acknowledge the financial support from Program of Pharmacy, Faculty of Science and Technology, Ma Chung University. This study was supported by Parasitology Laboratory, Faculty of Medicine, Gadjah Mada University.

REFERENCES

1. Strobel, G.A., 2003. Endophytes as sources of bioactive products. *Microbes Infect.*, 5: 535-544.
2. Tanaka, M., H. Sukiman, M. Takebayashi, K. Saito and M. Suto *et al.*, 1999. Isolation, screening and phylogenetic identification of endophytes from plants in hokkaido Japan and java Indonesia. *Microb. Environ.*, 14: 237-241.

3. Ruch, R.J., S.J. Cheng and J.E. Klaunig, 1989. Prevention of cytotoxicity and inhibition of intercellular communication by antioxidant catechins isolated from Chinese green tea. *Carcinogenesis*, 10: 1003-1008.
4. Kandavel, D. and S. Sekar, 2015. Endophytic fungi from *Phyllanthus amarus* Schum. and Thonn. Capable of producing phyllanthin, hypophyllanthin and/or related compounds. *Int. J. Pharm. Pharmaceut. Sci.*, 7: 253-257.
5. Richardson, S.N., T.K. Nsiama, A.K. Walker, D.R. McMullin and J.D. Miller, 2015. Antimicrobial dihydrobenzofurans and xanthenes from a foliar endophyte of *Pinus strobus*. *Phytochemistry*, 117: 436-443.
6. Gnani, G., F.P. Esposito, C. Festa, A. Poli and P. Tedesco *et al.*, 2016. The antimicrobial potential of algicolous marine fungi for counteracting multidrug-resistant bacteria: Phylogenetic diversity and chemical profiling. *Res. Microbiol.*, 167: 492-500.
7. Na, R., L. Jiajia, Y. Dongliang, P. Yingzi and H. Juan *et al.*, 2016. Identification of vincamine indole alkaloids producing endophytic fungi isolated from *Nerium indicum*, Apocynaceae. *Microbiol. Res.*, 192: 114-121.
8. Raj, K.G., R. Manikandan, C. Arulvasu and M. Pandi, 2015. Anti-proliferative effect of fungal taxol extracted from *Cladosporium oxysporum* against human pathogenic bacteria and human colon cancer cell line HCT 15. *Spectrochim. Acta Part A: Mol. Biomol. Spectrosc.*, 138: 667-674.
9. Egan, J.M., A. Kaur, H.A. Raja, J.J. Kellogg, N.H. Oberlies and N.B. Cech, 2016. Antimicrobial fungal endophytes from the botanical medicine goldenseal (*Hydrastis canadensis*). *Phytochem. Lett.*, 17: 219-225.
10. Sowparthani, K. and G. Kathiravan, 2010. *In-vitro* antibacterial screening of ethyl acetate extract endophytic fungi isolated from *Phyllanthus amarus* (Schum and Thonn) against pathogenic bacterial strains. *J. Pharmaceut. Biomed. Sci.*, 10: 1-4.
11. Paithankar, V.V., K.S. Raut, R.M. Charde and J.V. Vyas, 2015. *Phyllanthus niruri*. A magic herb. *Res. Pharm.*, 1: 1-9.
12. Hariono, M., H.A. Wahab, M.L. Tan, M.M. Rosli and I.A. Razak, 2014. 9-Benzyl-6-benzylsulfanyl-9H-purin-2-amine. *Acta Crystallogr. Sect. E: Struct. Rep.*, 70: o288-o288.
13. Colpo, E., C.D.D.A. Vilanova, R.P. Pereira, L.G.B. Reetz and L. Oliveira *et al.*, 2014. Antioxidant effects of *Phyllanthus niruri* tea on healthy subjects. *Asian Pacif. J. Trop. Med.*, 7: 113-118.
14. Mediani, A., F. Abas, A. Khatib, C.P. Tan and I.S. Ismail *et al.*, 2015. Relationship between metabolites composition and biological activities of *Phyllanthus niruri* extracts prepared by different drying methods and solvents extraction. *Plant Foods Human Nutr.*, 70: 184-192.
15. Coates, A., Y. Hu, R. Bax and C. Page, 2002. The future challenges facing the development of new antimicrobial drugs. *Nat. Rev. Drug Discov.*, 1: 895-910.
16. Sies, H., 1997. Oxidative stress: Oxidants and antioxidants. *Exp. Physiol.*, 82: 291-295.
17. Mans, D.R.A., A.B. da Rocha and G. Schwartzmann, 2000. Anti-cancer drug discovery and development in Brazil: Targeted plant collection as a rational strategy to acquire candidate anti-cancer compounds. *Oncologist*, 5: 185-198.
18. Kumar, S., N. Kaushik, R. Edrada-Ebel, R. Ebel and P. Proksch, 2011. Isolation, characterization and bioactivity of endophytic fungi of *Tylophora indica*. *World J. Microb. Biotechnol.*, 27: 571-577.
19. White, T.J., T.D. Bruns, S.B. Lee and J.W. Taylor, 1990. Amplification and Direct Sequencing of Fungal Ribosomal RNA Genes for Phylogenetics. In: *PCR Protocols: A Guide to Methods and Applications*, Innis, M.A., D.H. Gelfand, J.J. Sninsky and T.J. White (Eds.). Academic Press, San Diego, CA., USA., ISBN-13: 9780123721808, pp: 315-322.
20. O'Donnell, K., 1992. *Fusarium* and its near relatives. The fungal holomorph: Mitotic, meiotic and pleomorphic speciation in fungal systematics. *Proceedings of the International Symposium, August 4-7, 1992, Newport, Oregon*, pp: 226-233.
21. Hiraishi, A., Y. Kamagata and K. Nakamura, 1995. Polymerase chain reaction amplification and restriction fragment length polymorphism analysis of 16S rRNA genes from methanogens. *J. Ferment. Bioeng.*, 79: 523-529.
22. Hudzicki, J., 2009. Kirby-Bauer disk diffusion susceptibility test protocol. *ASM Microbe Library, American Society for Microbiology, Washington, DC*.
23. Schwarz, S., P. Silley, S. Simjee, N. Woodford, E. van Duijkeren, A.P. Johnson and W. Gastra, 2010. Editorial: Assessing the antimicrobial susceptibility of bacteria obtained from animals. *J. Antimicrob. Chemother.*, 65: 601-604.
24. Bressan, W. and M.T. Borges, 2004. Delivery methods for introducing endophytic bacteria into maize. *BioControl*, 49: 315-322.
25. Singleton, V.L. and J.A. Rossi Jr., 1965. Colorimetry of total phenolics with phosphomolybdic-phosphotungstic acid reagents. *Am. J. Enol. Viticult.*, 16: 144-158.
26. Oyaizu, M., 1986. Studies on products of browning reaction. Antioxidative activities of products of browning reaction prepared from glucosamine. *Jpn. J. Nutr. Dietetics*, 44: 307-315.
27. Hayon, T., A. Dvilansky, O. Shpilberg and I. Nathan, 2003. Appraisal of the MTT-based assay as a useful tool for predicting drug chemosensitivity in leukemia. *Leukemia Lymphoma*, 44: 1957-1962.
28. Sharma, O., 1989. *Textbook of Fungi*. Tata McGraw-Hill Education, New York, USA., ISBN: 9780074603291, Pages: 365.
29. Ares, M., 2012. Bacterial RNA isolation. *Cold Spring Harb. Prot.*, 9: 1024-1027.

30. Karey, K.P. and D.A. Sirbasku, 1988. Differential responsiveness of human breast cancer cell lines MCF-7 and T47D to growth factors and 17 β -estradiol. *Cancer Res.*, 48: 4083-4092.
31. Ross, J.S., G.P. Linette, J. Stec, M.S. Ross, S. Anwar and A. Boguniewicz, 2003. DNA ploidy and cell cycle analysis in breast cancer. *Am. J. Clin. Pathol.*, 120: S72-84.
32. Falck, J., N. Mailand, R.G. Syljuasen, J. Bartek and J. Lukas, 2001. The ATM-Chk2-Cdc25A checkpoint pathway guards against radioresistant DNA synthesis. *Nature*, 410: 842-847.
33. Mailand, N., J. Falck, C. Lukas, R.G. Syljuasen, M. Welcker, J. Bartek and J. Lukas, 2000. Rapid destruction of human Cdc25A in response to DNA damage. *Science*, 288: 1425-1429.
34. Costanzo, V., K. Robertson, C.Y. Ying, E. Kim and E. Avvedimento *et al.*, 2000. Reconstitution of an ATM-dependent checkpoint that inhibits chromosomal DNA replication following DNA damage. *Mol. Cell*, 6: 649-659.
35. Kim, G.Y., S.E. Mercer, D.Z. Ewton, Z. Yan, K. Jin and E. Friedman, 2002. The stress-activated protein kinases p38 α and JNK1 stabilize p21^{Cip1} by phosphorylation. *J. Biol. Chem.*, 277: 29792-29802.
36. Goloudina, A., H. Yamaguchi, D.B. Chervyakova, E. Appella, A.J. Fornace Jr. and D.V. Bulavin, 2003. Regulation of human Cdc25A stability by serine 75 phosphorylation is not sufficient to activate a S-phase checkpoint. *Cell Cycle*, 2: 471-476.
37. Di Leo, A., M. Tanner, C. Desmedt, M. Paesmans and F. Cardoso *et al.*, 2007. p-53 gene mutations as a predictive marker in a population of advanced breast cancer patients randomly treated with doxorubicin or docetaxel in the context of a phase III clinical trial. *Ann. Oncol.*, 18: 997-1003.
38. Vayssade, M., H. Haddada, L. Faridoni Laurens, S. Tourpin, A. Valent, J. Benard and J.C. Ahomadegbe, 2005. P73 functionally replaces p53 in Adriamycin treated, p53 deficient breast cancer cells. *Int. J. Cancer*, 116: 860-869.
39. Eastman, A., E.A. Kohn, M.K. Brown, J. Rathman, M. Livingstone, D.H. Blank and G.W. Gribble, 2002. A novel indolocarbazole, ICP-1, abrogates DNA damage-induced cell cycle arrest and enhances cytotoxicity: Similarities and differences to the cell cycle checkpoint abrogator UCN-01 1 supported by NIH Grant CA82220 and cancer center support grant CA23108 to the norris cotton cancer center. E. A. K. was supported by a fellowship from the Susan G. Komen breast cancer foundation. *Mol. Cancer Therapeutics*, 1: 1067-1078.
40. Ma, C.X., J.W. Janetka and H. Piwnicka-Worms, 2011. Death by releasing the breaks: CHK1 inhibitors as cancer therapeutics. *Trends Mol. Med.*, 17: 88-96.
41. Wang, Y., J. Li, R.N. Booher, A. Kraker, T. Lawrence, W.R. Leopold and Y. Sun, 2001. Radiosensitization of p53 mutant cells by PD0166285, a novel G₂ checkpoint abrogator. *Cancer Res.*, 61: 8211-8217.
42. Zabludoff, S.D., C. Deng, M.R. Grondine, A.M. Sheehy and S. Ashwell *et al.*, 2008. AZD7762, a novel checkpoint kinase inhibitor, drives checkpoint abrogation and potentiates DNA-targeted therapies. *Mol. Cancer Therapeutics*, 7: 2955-2966.
43. Zhang, G., V. Gurtu, S.R. Kain and G. Yan, 1997. Early detection of apoptosis using a fluorescent conjugate of annexin V. *Biotechniques*, 23: 525-531.
44. Schafer, J.M., E.S. Lee, R.M. O'Regan, K. Yao and V.C. Jordan, 2000. Rapid development of tamoxifen-stimulated mutant p53 breast tumors (T47D) in athymic mice. *Clin. Cancer Res.*, 6: 4373-4380.
45. Mokhtari, M.J., A. Akbarzadeh, M. Hashemi, G. Javadi and R. Mahdian *et al.*, 2012. Cisplatin induces down regulation of Bcl2 in T47D Breast cancer cell line. *Adv. Stud. Biol.*, 4: 19-25.
46. Jamieson, E.R. and S.J. Lippard, 1999. Structure, recognition and processing of cisplatin-DNA adducts. *Chem. Rev.*, 99: 2467-2498.
47. Biswas, S.K., J. Huang, S. Persaud and A. Basu, 2004. Down-regulation of Bcl-2 is associated with cisplatin resistance in human small cell lung cancer H69 cells. *Mol. Cancer Therapeutics*, 3: 327-334.
48. Leeson, P., 2012. Drug discovery: Chemical beauty contest. *Nature*, 481: 455-456.
49. Baars, L., 2007. Protein targeting, translocation and insertion in *Escherichia coli*: Proteomic analysis of substrate-pathway relationships. Ph.D. Thesis, Stockholm University, Sweden.
50. Kemp, L.E., C.S. Bond and W.N. Hunter, 2003. Structure of a tetragonal crystal form of *Escherichia coli* 2-C-methyl-D-erythritol 4-phosphate cytidyltransferase. *Acta Crystallographica Section D: Biol. Crystallography*, 59: 607-610.
51. Mascarenhas, N.M. and J. Kastner, 2013. How maltose influences structural changes to bind to maltose binding protein: Results from umbrella sampling simulation. *Proteins: Struct. Function Bioinform.*, 81: 185-198.
52. McKnight, G.L., S.L. Mudri, S.L. Mathewes, R.R. Traxinger, S. Marshall, P.O. Sheppard and P.J. O'Hara, 1992. Molecular cloning, cDNA sequence and bacterial expression of human glutamine: Fructose-6-phosphate amidotransferase. *J. Biol. Chem.*, 267: 25208-25212.
53. Dover, S. and Y.S. Halpern, 1972. Utilization of γ -aminobutyric acid as the sole carbon and nitrogen source by *Escherichia coli* K-12 mutants. *J. Bacteriol.*, 109: 835-843.
54. Brvar, M., A. Perdih, M. Renko, G. Anderluh, D. Turk and T. Solmajer, 2012. Structure-based discovery of substituted 4, 5'-bithiazoles as novel DNA gyrase inhibitors. *J. Med. Chem.*, 55: 6413-6426.

55. Seefeld, M.A., W.H. Miller, K.A. Newlander, W.J. Burgess and D.J. Payne *et al.*, 2001. Inhibitors of bacterial enoyl acyl carrier protein reductase (FabI): 2, 9-disubstituted 1, 2, 3, 4-tetrahydropyrido [3, 4-b] indoles as potential antibacterial agents. *Bioorganic Med. Chem. Lett.*, 11: 2241-2244.
56. Nakama, T., O. Nureki and S. Yokoyama, 2001. Structural basis for the recognition of isoleucyl-adenylate and an antibiotic, mupirocin, by isoleucyl-tRNA synthetase. *J. Biol. Chem.*, 276: 47387-47393.
57. Hayashi, H., H. Mizuguchi, I. Miyahara, Y. Nakajima, K. Hirotsu and H. Kagamiyama, 2003. Conformational change in aspartate aminotransferase on substrate binding induces strain in the catalytic group and enhances catalysis. *J. Biol. Chem.*, 278: 9481-9488.
58. Gil-Ortiz, F., S. Ramon-Maiques, I. Fita and V. Rubio, 2003. The course of phosphorus in the reaction of N-acetyl-l-glutamate kinase, determined from the structures of crystalline complexes, including a complex with an AlF₄ transition state mimic. *J. Mol. Biol.*, 331: 231-244.
59. Schmitt, E., Y. Mechulam, M. Fromant, P. Plateau and S. Blanquet, 1997. Crystal structure at 1.2 Å resolution and active site mapping of *Escherichia coli* peptidyl tRNA hydrolase. *EMBO J.*, 16: 4760-4769.
60. Davidson, A.L., H.A. Shuman and H. Nikaido, 1992. Mechanism of maltose transport in *Escherichia coli*: Transmembrane signaling by periplasmic binding proteins. *Proc. Nat. Acad. Sci.*, 89: 2360-2364.
61. Patrick, G.L., 2013. *An Introduction to Medicinal Chemistry*. Oxford University Press, USA., ISBN: 9780199697397, Pages: 789.
62. Eldar, A., H. Rozenberg, Y. Diskin-Posner, R. Rohs and Z. Shakked, 2013. Structural studies of p53 inactivation by DNA-contact mutations and its rescue by suppressor mutations via alternative protein-DNA interactions. *Nucleic Acids Res.*, 41: 8748-8759.
63. Rautureau, G.J.P., M. Yabal, H. Yang, D.C.S. Huang, M. Kvensakul and M.G. Hinds, 2012. The restricted binding repertoire of Bcl-2 leaves Bim as the universal BH3-only prosurvival Bcl-2 protein antagonist. *Cell Death Dis.*, Vol. 3. 10.1038/cddis.2012.178.
64. Liu, J., A. Sudom, X. Min, Z. Cao and X. Gao *et al.*, 2012. Structure of the nuclear factor κB-inducing kinase (NIK) kinase domain reveals a constitutively active conformation. *J. Biol. Chem.*, 287: 27326-27334.
65. Getlik, M., C. Grutter, J.R. Simard, S. Kluter and M. Rabiller *et al.*, 2009. Hybrid compound design to overcome the gatekeeper T338M mutation in cSrc#. *J. Med. Chem.*, 52: 3915-3926.
66. Ravelli, R.B.G., B. Gigant, P.A. Curmi, I. Jourdain, S. Lachkar, A. Sobel and M. Knossow, 2004. Insight into tubulin regulation from a complex with colchicine and a stathmin-like domain. *Nature*, 428: 198-202.
67. Warnmark, A., E. Treuter, J.A. Gustafsson, R.E. Hubbard, A.M. Brzozowski and A.C. Pike, 2002. Interaction of transcriptional intermediary factor 2 nuclear receptor box peptides with the coactivator binding site of estrogen receptor alpha. *J. Biol. Chem.*, 277: 21862-21868.
68. Thoma, R., T. Schulz-Gasch, B. D'Arcy, J. Benz and J. Aebi *et al.*, 2004. Insight into steroid scaffold formation from the structure of human oxidosqualene cyclase. *Nature*, 432: 118-122.
69. Shiau, A.K., D. Barstad, P.M. Loria, L. Cheng, P.J. Kushner, D.A. Agard and G.L. Greene, 1998. The structural basis of estrogen receptor/coactivator recognition and the antagonism of this interaction by tamoxifen. *Cell*, 95: 927-937.
70. Namboodiri, H.V., M. Bukhtiyarova, J. Ramcharan, M. Karpusas, Y. Lee and E.B. Springman, 2010. Analysis of imatinib and sorafenib binding to p38alpha compared with c-Abl and b-Raf provides structural insights for understanding the selectivity of inhibitors targeting the DFG-out form of protein kinases. *Biochemistry*, 49: 3611-3618.
71. Mezzetti, A., J.D. Schrag, C.S. Cheong and R.J. Kazlauskas, 2005. Mirror-image packing in enantiomer discrimination molecular basis for the enantioselectivity of *B. cepacia* lipase toward 2-methyl-3-phenyl-1-propanol. *Chem. Biol.*, 12: 427-437.
72. Ghosh, D., W. Jiang, J. Lo and C. Egbuta, 2011. Higher order organization of human placental aromatase. *Steroids*, 76: 753-758.
73. Fajardo-Dolci, G., R. Gutierrez-Vega, H. Arboleya-Casanova, A. Villalobos and K.S. Wilson, 2010. Clinical characteristics of fatalities due to influenza A (H1N1) virus in Mexico. *Thorax*, 65: 505-509.